Unrepaired clustered DNA lesions induce chromosome breakage in human cells

Aroumougame Asaithamby[1], Burong Hu[2], and David J. Chen[1]

Division of Molecular Radiation Biology, Department of Radiation Oncology, University of Texas Southwestern Medical Center, Dallas, TX 75390

Edited by Susan S. Wallace, University of Vermont, Burlington, VT, and accepted by the Editorial Board April 1, 2011 (received for review October 25, 2010)

Clustered DNA damage induced by ionizing radiation is refractory to repair and may trigger carcinogenic events for reasons that are not well understood. Here, we used an in situ method to directly monitor induction and repair of clustered DNA lesions in individual cells. We showed, consistent with biophysical modeling, that the kinetics of loss of clustered DNA lesions was substantially compromised in human fibroblasts. The unique spatial distribution of different types of DNA lesions within the clustered damages, but not the physical location of these damages within the subnuclear domains, determined the cellular ability to repair the damage. We then examined checkpoint arrest mechanisms and yield of gross chromosomal aberrations. Induction of nonrepairable clustered damage affected only G2 accumulation but not the early G2/M checkpoint. Further, cells that were released from the G2/M checkpoint with unrepaired clustered damage manifested a spectrum of chromosome aberrations in mitosis. Difficulties associated with clustered DNA damage repair and checkpoint release before the completion of clustered DNA damage repair appear to promote genome instability that may lead to carcinogenesis.

heterochromatin | high linear energy transfer | high charge and energy particles | 53BP1 | ionizing radiation induced foci

Ionizing radiation (IR) may induce cancer and loss of neural function or death in humans. Low (e.g., γ- and X-rays) and high [i.e., high charge and energy (HZE)] linear energy transfer (LET) IR induces a plethora of DNA damage, and the damage complexity increases with an increase in the LET of the radiation (1–3). Isolated DNA lesions (mainly induced by low-LET radiation), including double-strand breaks (DSBs), single-strand breaks (SSBs), and damaged bases located at a distance from other damage, are generally repaired efficiently. Substantial evidence indicates that high-LET radiation induces complex DNA damage, a unique class of DNA lesions that includes two or more individual lesions within one or two helical turns of the DNA (4). These lesions can be abasic sites (apurinic/apyrimidinic sites or APs), damaged bases (oxidized purines or pyrimidines), SSBs, or DSBs (5). Convincing evidence indicates that complex DNA lesions are more difficult to repair than isolated lesions and in some instances are irreparable; however, it is unclear why clustered lesions are difficult to repair.

The biological consequences of complex DNA damage range from point mutations and loss of genetic material to cellular lethality due to repair impairment and lesion or repair-intermediate persistency. Clustered lesions induce intra- and interchromosomal insertions, and inversions often in association with large deletions (6). FISH-painting methodologies were used to show that high-LET IR induces a high fraction of chromosome rearrangements (7). Recently, it has been suggested that non-DSB clusters, if unrepaired, can lead to the formation of mutations and chromosome abnormalities (8). After exposure to high-LET radiation, immortalized human bronchial (BEP2D) and breast (MCF-10F) cells undergo malignant transformation and become tumorigenic in nude mice (9). Recently, it was found in a mouse model that high-LET IR treatment results in tumors with significantly higher frequency and shorter latency compared with tumors generated by low-LET IR (10). The mechanism by which these lesions trigger carcinogenic events is unknown.

Biophysical modeling, in vitro biochemical assays with phage or plasmid DNA, and in vivo assays in mammalian cells and in animals have been used to estimate induction and repair of clustered DNA damages. These methods provide only an indication of the average numbers of different types DNA lesions but do not reveal the subcellular localization, dynamics of DNA repair, or spatial relationships of lesions. To directly visualize the induction and repair of clustered DNA lesions at the single-cell level, we used immunofluorescence staining of repair proteins as surrogate markers to examine DSBs, SSBs and base damage in human cells. Our results show that a large fraction of 53BP1, XRCC1, and hOGG1 foci colocalized with another marker in cells irradiated with iron (Fe) and silicon (Si) ions, suggesting that the majority of the lesions were complex in nature. Most clustered DNA damage was irreparable in Fe ion-irradiated cells. Further, the volume of 53BP1, XRCC1, and hOGG1 foci colocalization was significantly higher in cells exposed to Fe ions than Si ions. We also showed that cells released from the G2/M checkpoint enter mitosis with unrepaired clustered lesions, which results in the formation of chromosomal aberrations.

Results

Direct Visualization of Clustered DNA Lesions at the Single-Cell Level Using 53BP1, XRCC1, and hOGG1 as Surrogate Markers for DSBs, SSBs, and Base Damage, Respectively, Reveals That Most Complex DNA Damage Is Not Repaired in Human Cells. Previously we reported that Si ion-induced DNA damage was repaired in a manner similar to repair of γ-ray-induced damage and that a larger fraction of Fe ion-induced DNA damage was irreparable (11). The difficulties associated with repair of DNA lesions induced by irradiation with Fe ions may be due to either the number of complex DNA lesions produced or the nature of clustered lesions induced. We first evaluated whether the DNA damage induced by Fe ions were quantitatively different from that induced by Si ions. Human fibroblasts stably expressing the SSB marker EGFP-XRCC1 were irradiated with 1 Gy of Si (LET 44 keV/μm) or Fe (LET 150 keV/μm) ions. We used fluorescently tagged XRCC1 and immunofluorescence staining of 53BP1 and hOGG1 as surrogate markers for SSBs, DSBs, and base damage, respectively (for further discussion of these markers, see *SI Text*). Examination of high-resolution deconvoluted images for 53BP1, XRCC1, and hOGG1 foci revealed that both the ions induced all three types of DNA lesions (Fig. 1*A* and Fig. S1*A*). A large fraction of 53BP1, XRCC1, and hOGG1 foci were colocalized with another marker, suggesting that the majority of the lesions were complex

Author contributions: A.A. and D.J.C. designed research; A.A. and B.H. performed research; D.J.C. contributed new reagents/analytic tools; A.A., B.H., and D.J.C. analyzed data; and A.A. wrote the paper.

The authors declare no conflict of interest.

This article is a PNAS Direct Submission. S.S.W. is a guest editor invited by the Editorial Board.

Freely available online through the PNAS open access option.

[1]To whom correspondence may be addressed. E-mail: david.chen@utsouthwestern.edu or aroumougame.asaithamby@utsouthwestern.edu.

[2]Present address: Key Laboratory of Heavy Ion Radiation Biology and Medicine, Institute of Modern Physics, Chinese Academy of Sciences, Lanzhou, China.

This article contains supporting information online at www.pnas.org/lookup/suppl/doi:10.1073/pnas.1016045108/-/DCSupplemental.

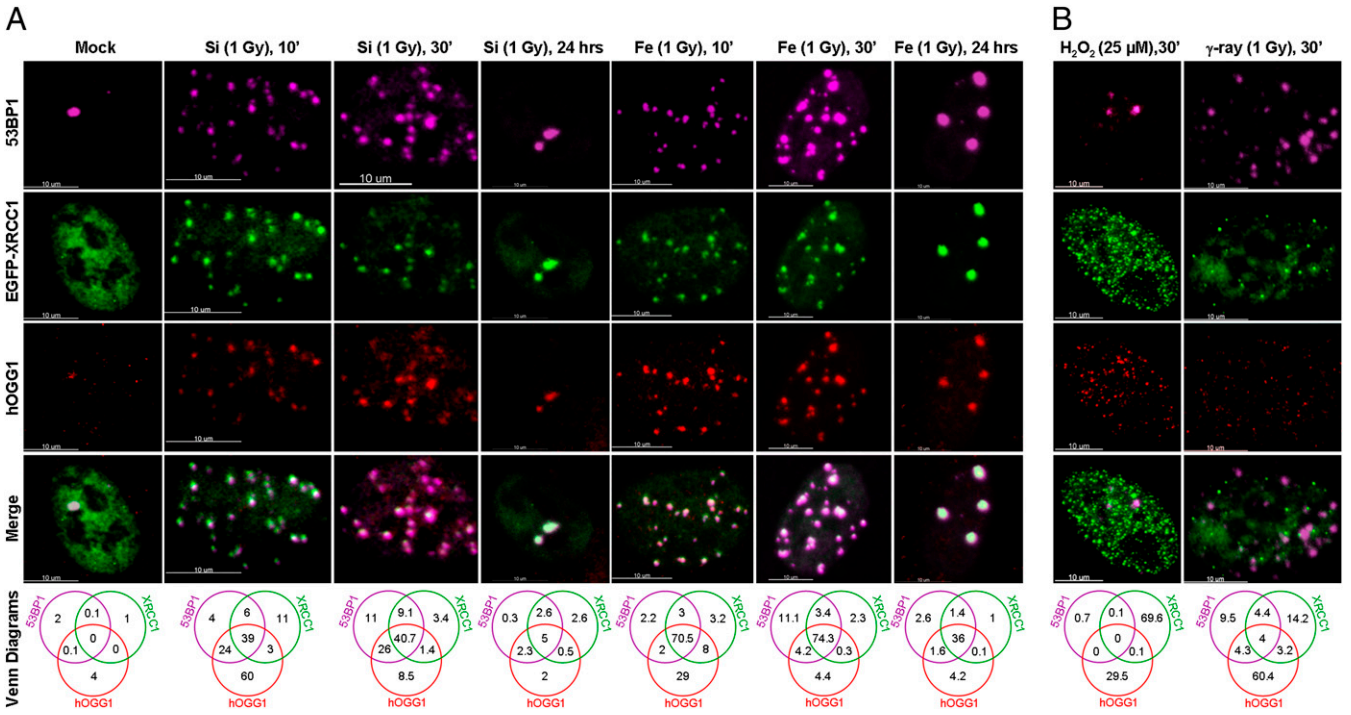

Fig. 1. Clustered DNA damage induced by Fe ions but not by Si ions is refractory to repair. (*A Upper*) Representative images show recruitment and retention of 53BP1, EGFP-XRCC1, and hOGG1 at the sites of DNA damage induced by 1 Gy of Si or Fe ions. (*A Lower*) Venn diagrams show percentage of individual and colocalized 53BP1, EGFP-XRCC1, and hOGG1 foci at indicated times after irradiation. Data shown are the percentage of foci relative to the number in cell irradiated for 30 min (the sum of 53BP1, EGFP-XRCC1, and hOGG1 foci numbers at 30 min was defined as 100%). (*B*) H_2O_2 does not induce clustered DNA damage and γ-rays induce only a small number of clustered DNA lesions. (*Upper*) Representative images show induction of 53BP1, EGFP-XRCC1, and hOGG1 foci in cells treated with 25 mM H_2O_2 or 1 Gy γ-rays at 30 min after exposure. (*Lower*) Venn diagrams show percentages of colocalized foci (calculated as in *A*). HT1080 cells stably expressing EGFP-XRCC1 were treated with different DNA damaging agents, immunostained with anti-53BP1 and hOGG1 antibodies, and the images were recorded using confocal microscopy. In each experiment, the average of individual and colocalized foci in 100–120 cells from two to three independent experiments was used for the calculation. More details are provided in *SI Text*).

in nature. To quantify these findings, we estimated the number of individual and colocalized foci using 3D imaging technology. As shown in the Venn diagrams in Fig. 1*A*, the percent of individual as well as colocalized foci differed significantly between 30 min and 24 h after irradiation and also between cells exposed to Si and Fe ions. At 30 min after irradiation, complex DNA damage (i.e., two or three overlapping markers) comprised ∼70–85% of lesions, suggesting that both ions induced similar levels of complex DNA lesions. However, in the majority of Fe ion-generated lesions (∼70–74%), all three markers colocalized, whereas only ∼40% of Si-induced lesions stained for all three markers. Significantly higher numbers of foci persisted in Fe ion-irradiated cells than in Si-treated cells at 24 h (Fig. 1*A*). Strikingly, in the majority of lesions that persisted in Fe ion-irradiated cells, all three markers were colocalized. Further, the kinetics of disappearance of foci stained with all three markers was slower in cells irradiated with Fe ions than in those treated with Si ions. Mathematical modeling of foci dissolution kinetics data supported this conclusion (Table S1). Nonlinear dynamic fitting of foci dissolution kinetics showed that ∼70% of foci were repaired with slow kinetics in Fe ion-irradiated cells, whereas only 27% were repaired slowly in Si ion-irradiated cells. Collectively, these data demonstrate that Fe ion-induced damage was repaired with slower kinetics than Si ion-induced damage, and much of the Fe ion-induced damage was not repaired.

To exclude the possibility that the colocalization of 53BP1, XRCC1, and hOGG1 foci was a result of fusion or contact of different IR-induced foci (IRIF) due to chromatin dynamics during DNA repair (12), we quantitated the individual as well as colocalized 53BP1, XRCC1, and hOGG1 foci immediately after irradiation (Fig. 1*A* and Fig. S1*A*). We found that at 10 min after IR, ∼40% and 70% of 53BP1, XRCC1, and hOGG1 foci were colocalized in Si and Fe ion-irradiated cells, respectively. These percentages are similar to those measured at 30 min after IR. Thus, this observation confirms that the colocalization of 53BP1, XRCC1, and hOGG1 foci represents the sites of clustered DNA damage and that the foci colocalization was not due to fusion or contact of different IRIF due to the radiation-induced chromatin dynamics during DNA repair.

To further exclude the possibility that the colocalization of 53BP1, XRCC1, and hOGG1 foci in irradiated cells was due to IRIF spread (13–15), we carefully examined the individual as well as colocalized 53BP1, XRCC1, and hOGG1 foci in cells treated with 25 μM hydrogen peroxide (H_2O_2) or with 1 Gy of γ-rays (Fig. 1*B* and Fig. S1*B*). Examination of high-resolution deconvoluted images for 53BP1, XRCC1, and hOGG1 foci revealed that both H_2O_2 and γ-rays induced all three types of DNA lesions (Fig. 1*B*), and almost all these foci disappeared after 24 h (Fig. S1*B*). Importantly, we did not observe any colocalization of 53BP1, XRCC1, and hOGG1 foci after the H_2O_2 treatment (Fig. 1*B* and Fig. S1*B*). In contrast to H_2O_2, ∼18–20% of 53BP1, XRCC1, and hOGG1 foci were colocalized with another marker in γ-irradiated cells (Fig. 1*B* and Fig. S1*B*). Together these results confirm that the colocalized 53BP1, XRCC1, and hOGG1 foci in Fe and Si ion-irradiated cells represent the sites of clustered DNA damage and that the foci colocalization is not due to IRIF spread on the DNA molecule.

A Unique Spatial Distribution of Different Types of DNA Lesions Within the Clustered DNA Damage Determines the Efficiency of Complex DNA Damage Repair in Cells. Unlike Si ion-induced damage, most complex DNA damage induced by Fe ions was irreparable which may be due to either the generation of greater density of different types of lesions within the clustered lesions or

the physical location of the damage within the nuclear subdomains. We examined the spatial distribution of DSB, SSB, and damaged base markers within the complex DNA lesions using a cytological imaging approach (Fig. 2 and Table S2). In general, there was close overlap among 53BP1, XRCC1, and hOGG1 markers, and the XRCC1 and hOGG1 markers assembled near the center of the complex DNA lesions and were surrounded by larger regions of 53BP1 staining (Fig. 2*A*). To quantify these findings, we measured the volume of overlap among 53BP1, XRCC1, and hOGG1 markers along the densely ionized tracks traversed by these ions using a 3D imaging approach (Fig. 2*B*). Irradiation of cells with Fe ions resulted in a tight overlap (80%) between XRCC1 and hOGG1 markers and in tight colocalization of these two markers with 53BP1 (90%) at 10 min after irradiation (Fig. 2*B*). In contrast, at 10 min after Si ion irradiation, only ∼50% overlap was observed among 53BP1, XRCC1, and hOGG1 markers, and the levels of colocalization were significantly different from those of Fe ion-induced lesions. Interestingly, in foci induced by both Si and Fe ions that persisted in irradiated cells, both XRCC1 and hOGG1 markers showed a tight overlap (90%) but also exhibited a tight overlap with 53BP1 (90%; Fig. 2*B*). These data suggest that Fe ions induced complex DNA damage with greater density of different types of DNA lesions than did irradiation with Si ions. 3D modeling of spatial distribution of different markers supported this conclusion. As illustrated in Fig. 2*C*, the degree of overlap among different surrogate markers at the early time point was significantly different between Si and Fe ions, but differences were not significant at 24 h after irradiation. Evaluation of volume and area of each marker in individual IRIFs at 10 min after IR revealed that the volumes and areas of 53BP1, XRCC1, and hOGG1 foci in Fe ion-irradiated cells were larger than those in cells treated with Si ions (Table S2). Collectively, these results suggest that the difficulties associated with repair of clustered DNA damage in Fe-irradiated cells might be due to a tight spatial distribution of different types of DNA lesions within the clustered DNA damage.

Evidence suggests that chromatin organization regulates the cell's ability to repair DNA damage (14, 16–18). To elucidate whether inability to repair clustered DNA lesions is related to location within nuclear subdomains (i.e., euchromatin vs. heterochromatin), we examined colocalization of 53BP1 IRIF with a heterochromatin marker (Fig. 2 *D* and *E* and Fig. S2). We used only 53BP1 because the majority of the unrepaired lesions contained 53BP1 foci. Of all the initially induced and persistent 53BP1 foci, only a few were juxtaposed with heterochromatic regions (Fig. 2D and Fig. S2). Identical results were obtained with γ-rays, Si ions, and Fe ions. The fraction of heterochromatin-associated 53BP1 foci at 10 and 30 min after γ-ray, Si, or Fe irradiation ranged from two to six per cell. At 24 and 72 h after irradiation, 1–1.5 53BP1 foci per cell were associated with heterochromatin (Fig. 2*E*). These results demonstrated that most unrepaired lesions were found in euchromatin regions. Thus, difficulties associated with complex lesion repair were not due to their physical location within the subnuclear domains.

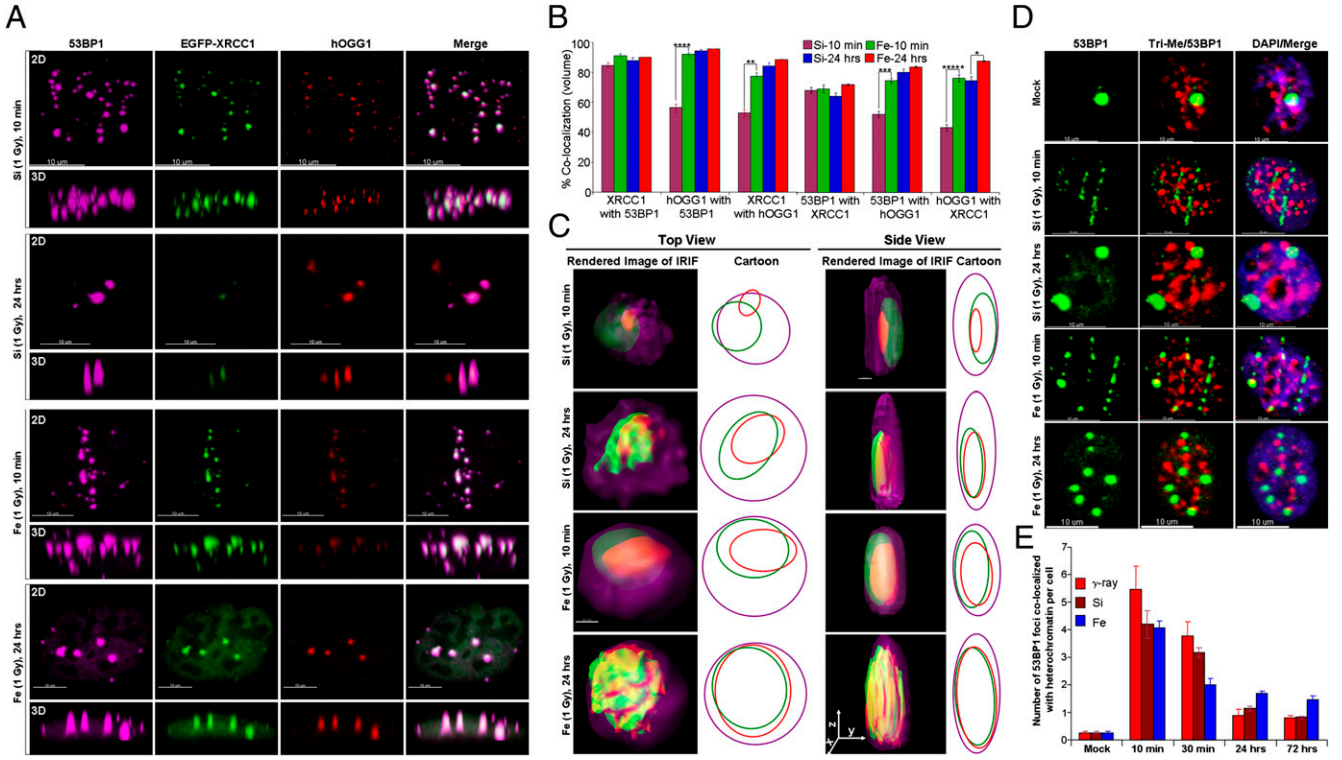

Fig. 2. Spatial distribution of DSBs, SSBs, and base lesions within the complex DNA damage determines the cellular ability to repair complex DNA damage. (*A*) 53BP1, XRCC1, and hOGG1 markers colocalize along the dense ionizing tracks traversed by Si and Fe ions. Representative 2D and 3D deconvoluted images show colocalization of 53BP1, XRCC1, and hOGG1 in cells treated with 1 Gy of Si or Fe ions. (*B*) 53BP1, XRCC1, and hOGG1 markers are tightly colocalized in Fe ion-irradiated cells. Graphs show levels of colocalization of different DNA lesion markers at 10 min and 24 h after 1 Gy of Si or Fe irradiation. Colocalization shown is the average obtained from 20 to 30 cells. Error bars represent SEM. **P* = 0.0001, ***P* = 0.2.3E-09, ****P* = 3.5E-10, *****P* = 1.4E-12, ******P* = 3.8E-13. (*C*) Fe ions induce very tight spatial distributions of DSB, SSB, and base lesions within the clustered DNA damage site. Representative illustration showing spatial colocalization of DSB, SSB, and damaged base markers within the clustered DNA damage induced by Si and Fe ions. (*D*) Not all persistent DNA lesions are associated with heterochromatic regions. Representative images show colocalization of 53BP1 with heterochromatic regions (Tri-Me) at indicated times after 1 Gy of Si or Fe ion irradiation. (*E*) The graph shows the number of 53BP1 foci that were juxtaposed with heterochromatic regions at indicated times after 1 Gy of γ-ray, Si, and Fe irradiation. The average number of colocalized foci in 100–120 cells from three independent experiments was used for the calculation. Error bars represent SEM. Detailed legend is provided in *SI Text*.

Unrepaired Clustered DNA Lesions Result in the Generation of a Spectrum of Chromosome Aberrations. To investigate how unrepaired clustered DNA damage results in carcinogenesis, we evaluated chromosomal aberrations in metaphase cells derived from cells treated with low- and high-LET irradiation. Classical chromosome analysis of metaphase spreads revealed that cells exposed to Fe ions had significantly ($P = 0.007$) elevated levels of chromosomal aberrations per mitotic cell relative to levels in mock-irradiated cells (Fig. 3*A*). The average number of aberrations per cell was ~2 for Fe ion-treated cells but was ~0.5 per cell for cells treated with Si ions, oxygen (O) ions, or γ-rays (Fig. 3*A*). Further, nearly 80% of Fe ion-irradiated cells exhibited at least one aberration, with the number of aberrations per cell ranging from one to six or more (Fig. S3*C*). The numbers of metaphases that produced aberrations and the numbers of aberrations per cells were lower in Si-, O-, and γ-ray-treated cells. These results clearly indicate that Fe ions induced significantly higher numbers of aberrations per cell in more cells than did other types of radiation. Although both low- and high-LET radiation induced a spectrum of chromatid and chromosomal aberrations, the extent was clearly dependent on the LET of the radiation (Fig. 3*B*). Higher numbers of aberrations, including chromatid breaks, triradial and quadriradial chromosomes, chromosomal breaks, dicentrics, and rings, were observed in Fe ion-irradiated cells than in cells treated with other forms of radiation. Thus, we observed a direct link between the numbers of unrepaired clustered lesions and the numbers of the chromosomal aberrations in cells. The genomic instability that results from these aberrations presumably facilitates the initiation of carcinogenesis.

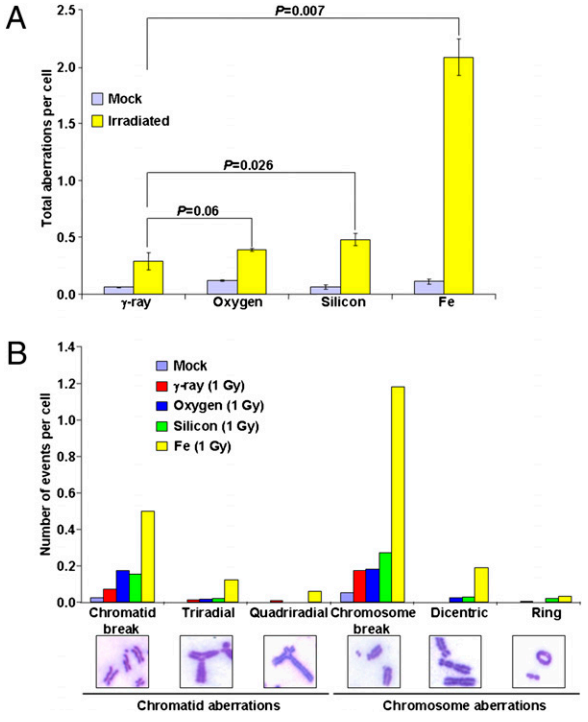

Fig. 3. Unrepaired clustered DNA lesions result in high levels of gross-chromosomal aberrations in Fe ion-irradiated cells. (*A*) The total number of gross chromosomal aberrations per mitotic cell. (*B*) The number of different types of chromosomal aberrations per mitotic cell after 1 Gy of γ-ray, O, Si, and Fe irradiation. Exponentially growing HT1080 cells were irradiated with 1 Gy of radiation, and 16 h later the chromosome preparations were made by accumulating mitotic cells in the presence of 0.1 mg/mL colcemid for 8 h. For each radiation type, more than 100 metaphase spreads were counted. Each data point in the graph is the average of three independent experiments. Error bars represent SD.

Checkpoint Release Before the Completion of Clustered DNA Damage Repair Is a Major Cause of Chromosomal Aberrations. An important question is why the levels of chromosome aberrations are elevated in Fe ion-irradiated cells relative to cells irradiated with lower levels of LET. Evidence suggests that the G2 checkpoint facilitates repair of chromosomal damage and that failure to arrest will lead to conversion of unrepaired DNA damage to chromosomal aberrations during the G2 to M phase transition (19, 20). To investigate the reason for the formation of increased levels of chromosomal aberrations in Fe ion-irradiated cells relative to cells treated with lower LET, we systematically examined induction and maintenance of the G2/M checkpoint using a combination of immunofluorescence and flow cytometry (Fig. 4). First, we evaluated late G2 accumulation by assessing the percentage of total cells with 4N DNA content by propidium iodide (PI) staining. Irradiated cells showed an increase in the G2/M population within first 8 h compared with mock-irradiated cells (Fig. 4 *A* and *B*). Twelve hours after γ-ray or Si ion irradiation, the number of G2/M cells returned to baseline. In contrast, cells irradiated with Fe ions exhibited a G2/M accumulation (Fig. 4 *A* and *B*). At 24 h after Fe ion irradiation, the number of G2/M cells returned to baseline. Similar results were obtained when immortalized human bronchial epithelial cells (HBECs) were examined (Fig. S4*A*). Thus, the length of G2/M arrest was directly proportional to the reparability of the clustered DNA damage.

Next, we used two-parameter flow cytometry to evaluate the early G2/M checkpoint using histone 3 phosphorylation (pH3) to distinguish mitotic cells from G2 cells (Fig. 4*C*). Although cells failed to enter into mitosis within the first 2 h after irradiation, they begin to enter mitosis after 4 h, and levels returned to the baseline by 12 h after irradiation (Fig. 4*C*). Interestingly, unlike the late G2/M accumulation, cells irradiated with Fe ions reentered mitosis at rates similar to cells irradiated with γ-rays and Si ions, demonstrating that the cessation of progression of cells from G2 into mitosis at early time points after irradiation was independent of the reparability of the clustered DNA damage. Thus, these data clearly suggest that, of the two stages of progression from G2 into mitosis (21), induction of repair-resistant cluster lesions by Fe ions affects only the late G2 checkpoint but not the early G2/M checkpoint.

To determine the cell-cycle stage of cells at the time of irradiation, cells were pulse-labeled with bromodeoxyuridine (BrdU) and then irradiated. Progression of cells through cell cycle was analyzed by flow cytometry at various time points after irradiation (Fig. 4*D* and Fig. S4*B*). The BrdU-labeled cells represent those in S phase at the time of irradiation. Cells accumulated in G2 over the next 4 h, and at 8 h after irradiation the percentage of BrdU-positive cells in the G2 phase peaked (Fig. 4*D*), demonstrating that the majority of the cells arrested were in the S phase at the time of irradiation. Significantly, Fe ion-irradiated cells, unlike those treated with γ-rays or Si ions, showed a prolonged arrest at the G2 phase. We evaluated the time course for the progression of S cells through G2, mitosis, and into G1 by analyzing the BrdU-labeled cells in G1 (Fig. 4*E*). The BrdU-positive cells escaped G2 and progressed back into the G1 phase of the cell cycle over 4 h, with the highest percentage of BrdU-positive cells in the G1 phase observed 12 h after irradiation (Fig. 4*E*). One major difference was that fewer BrdU-positive cells were released from G2/M and reentered G1 by 12 h after Fe ion irradiation than after lower-LET irradiation. This observation is consistent with the enhanced accumulation of G2/M seen with PI staining. Thus, these results demonstrate that the initiation event for G2/M accumulation actually occurs in the S phase of the cell cycle.

Although Fe ion-irradiated cells remained in the G2 phase of the cell cycle for a prolonged period relative to γ-ray- or Si-irradiated cells, the presence of BrdU-positive cells in the G1 phase (Fig. 4*E*) clearly suggests that the G2 accumulation was not a permanent arrest. Further, the presence of chromosomal aberrations in mitotic cells that were released from the G2 checkpoint arrest suggests that the release occurred before the

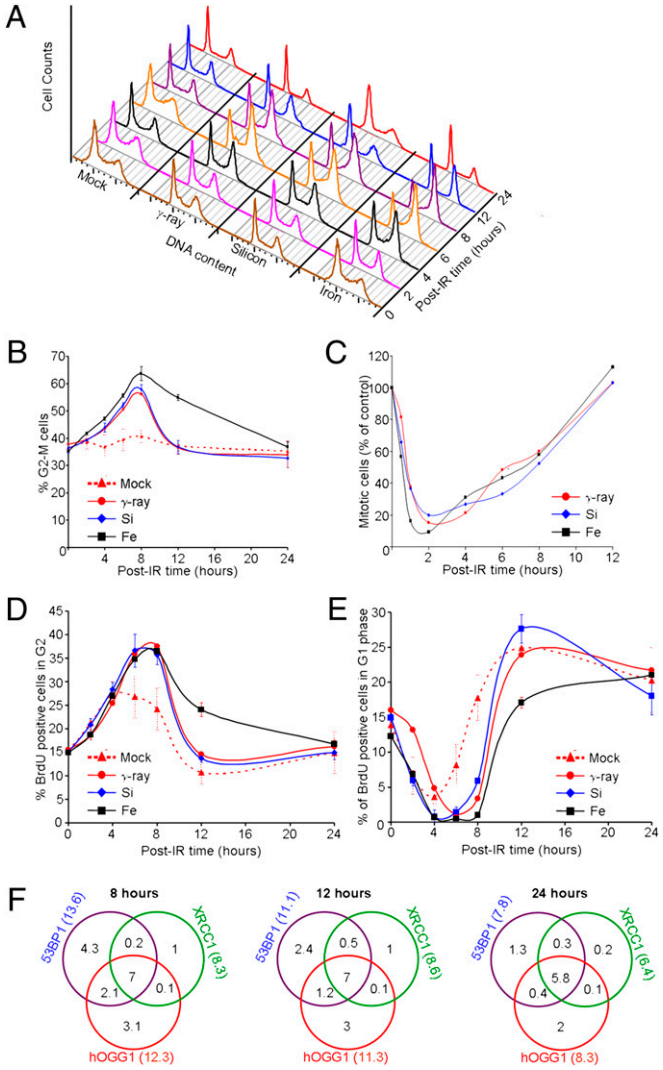

Fig. 4. Checkpoint release before the completion of clustered DNA damage repair represents a major cause for chromosome aberration formation. (*A*) Representative histograms show cell cycle profile at indicated times after mock treatment or 1 Gy of γ-ray, Si, or Fe irradiation. (*B*) The graph shows percentage of cells in G2/M phase at indicated times after mock-irradiation or 1 Gy of γ-ray, Si, or Fe irradiation. (*C*) The graph shows percentage of M phase cells relative to mock-irradiated cells at indicated times. (*D*) The graph shows percentage of BrdU-positive cells in G2 and (*E*). G1 phase cells at indicated times after mock-irradiation or treatment with 1 Gy of γ-rays or Si or Fe ions. For *D* and *E*, exponentially growing HT1080 cells were labeled with BrdU for 30 min and then irradiated with 1 Gy of Fe, Si, or O ions, or γ-rays. Subsequently, cells were immunostained with FITC-conjugated anti-BrdU antibody and then subjected to flow cytometry. (*F*) G2/M checkpoint release occurs before the completion of clustered DNA damage repair. Venn diagrams show number of individual and colocalized foci at indicated times after 1 Gy of Fe ion irradiation. More than 120 cells per time point from three independent experiments were examined. More details are provided in *SI Text*.

completion of clustered lesion repair. To further confirm that clustered lesion repair was incomplete at the point of checkpoint release, we evaluated the number of clustered lesions remaining during G2 arrest (8 and 12 h) and after G2/M release (24 h). There were about seven clustered DNA lesions per cell at 8- and 12-h time points and about six unrepaired lesions at 24 h in ~95% of Fe-irradiated cells (Fig. 4*F* and Fig. S5*A*). Thus, the G2 checkpoint was not maintained until the completion of lesion repair. There were fewer unrepaired clustered lesions in cells exposed to Si ions at 24 h than at 12 h (Fig. S5*B*). Together, these results clearly demonstrate that cells released from the G2 checkpoint do enter mitosis with unrepaired clustered lesions, which presumably results in formation of chromosomal aberrations.

Discussion

Recruitment and retention of DNA repair and response proteins at DNA breaks can be conveniently visualized by fluorescence imaging of repair foci, or IRIF. By using a fluorescently tagged XRCC1 and immunofluorescence staining of 53BP1 and hOGG1 as surrogate markers for SSBs, DSBs, and base damage, respectively, we demonstrated that the induction and repair of clustered DNA lesions can be directly visualized in individual cells. By using this in situ approach, we found that a large fraction of 53BP1, XRCC1, and hOGG1 foci colocalized in cells irradiated with Fe and Si ions, but not in H_2O_2-treated cells, suggesting that the colocalized IRIF represents the sites of clustered DNA lesions. Generally, a clustered DNA lesion is defined as two or more lesions formed within 1–2 helical turns of DNA by a single radiation track. Theoretical calculations predict that clustering of damage can occur both locally, over regions of up to 40 bp, and, owing to the organization of the chromatin as a 30-nm fiber, over regions extending several kilobases (22). Our data on the 53BP1, XRCC1, and hOGG1 foci volumes at 10 min after IR clearly suggest that the complex DNA damage is not confined within 1–2 helical turns of the DNA but, rather, as predicted by theoretical calculations, covers regions extending several kilobases of the DNA molecule. Further, both biophysical modeling and in vitro biochemical assays using hydrated plasmid DNA suggest that the yields of clustered DNA damage increase with increasing LET (2, 3, 23). Our in situ approach confirmed that the yields of clustered DNA damage increased with increasing LET. Our immunostaining approach does have some limitations. For example, each colocalized foci may not represent a single DNA lesion because of the optical limitations of the microscope. Therefore, the number of clustered DNA lesions we calculate may not be accurate. Cellular approaches in combination with in vitro assay systems will more precisely estimate the amount of clustered DNA lesions induced by HZE ions.

What makes repair of these complex DNA lesions so difficult? We envisaged two scenarios that might influence the cellular ability to repair complex DNA damage: the spatial distribution of different types of lesions within the clustered DNA damage and the physical location of damage within nuclear subdomains (euchromatic or heterochromatic). Monte Carlo simulation studies have predicted that the spatial density of the ionization or excitation along the track depends on the track structure or LET of the radiation (24). In cells treated with Si ions, damage was efficiently repaired, and the degree of colocalization of the three surrogate markers was moderate. In contrast, a majority of DNA lesions induced by Fe ions were repair resistant, and the degree of colocalization of the three damage markers was high. In addition, in foci that persisted, all three markers showed a very tight overlap. Therefore, it is reasonable to speculate that Fe ion-induced DNA lesions are very close to each other and that DNA lesions induced by Si ions are further apart. In vitro studies of oligonucleotides with defined lesions at specific relative spacings on opposing strands suggested that in two- or multiple-lesion clusters, the spatial arrangement of clusters is key in determining repair efficiency (25). Hence, it is possible that a tight spatial distribution of various lesions within the clustered DNA damage makes certain lesions inaccessible to repair enzymes (25).

Previous evidence suggested that DSBs repaired with slow kinetics predominantly localize to the periphery of the heterochromatin; thus, chromatin complexity may confer slow DSB repair kinetics (16, 17). Conversely, it was recently shown that the complexity of DNA lesions determines the speed of the repair (18). Similar to earlier findings (26), our data showed that, immediately after irradiation, a majority of the 53BP1 foci were located in the noncondensed DNA regions. Notably, we found that persistent damage in Fe ion-irradiated cells was localized in both heterochromatic and euchromatic regions. Thus, these data

clearly indicate that the efficiency of complex DNA lesions repair is dependent on the unique spatial distribution of different types of lesions within the clustered DNA damage site and is not due to the chromatin complexity.

Our classical chromosome analysis of metaphase spreads revealed that in cells exposed to Fe ions, the levels of chromosomal aberrations per mitotic cell were significantly elevated relative to mock-, Si-, O-, and γ-ray-irradiated cells. The levels of chromosomal abnormalities were clearly correlated with the extent of unrepaired DNA damage in these cells. The presence of high levels of chromosome aberrations in Fe-irradiated cells can be explained by the fact that the nonrepairable DSB clusters accumulate through DNA replication in S phase and chromatin condensation during G2- to M-phase transition and are converted and visualized at metaphase mainly as chromosome breaks. Furthermore, if chromatid breaks occur at two adjacent sites on two different chromosomes, asymmetrical or symmetrical quadriradial chromosomes are formed, depending on type of rejoining. As in other studies (15), our cell survival data showed that the differences in kinetics of lesion rejoining clearly affected the survival of the irradiated cells (Fig. S7*B* and *SI Text*). Although most irradiated cells died because of their inability to complete mitosis, some cells with repair-resistant DNA lesions survived and entered mitosis. Every round of replication is expected to increase the overall mutation level and lead to accumulation of mutations in surviving cells (27). Therefore, we believe that the biological significance of HZE ion-induced damage is high, because the accumulation of unrepaired DNA lesions combined with normal survival can provide the opportunity for genomic rearrangements and can increase genomic instability, leading to genetic changes required for progression from an initiated cell to a metastatic tumor cell (9, 10, 28).

The elevated levels of chromosomal aberrations in Fe ion-irradiated cells compared with those irradiated with lower-LET radiation might be due to induction of repair-resistant DNA lesions, an improperly functioning cell-cycle check point mechanism, or both. Their combined loss might be dramatic (28). The primary function of DNA damage checkpoints is to allow time for DNA damage repair. The loss of cell-cycle checkpoint arrest may allow damaged cells to proliferate. We found that Fe ion-irradiated cells are released from the G2/M checkpoint with unrepaired clustered DNA lesions and that these cells manifest chromosomal aberrations in mitosis. Similarly, it has been shown that in ataxia telangiectasia cells, radiation-induced G2/M checkpoint arrest is rapidly activated; however, release from G2 arrest occurs before the completion of DSB repair, resulting in chromosome breakage during mitosis (19, 20, 28). Thus, difficulties associated with clustered DNA lesion repair and checkpoint release before the completion of DNA repair contribute to the formation of chromosome aberrations (Fig. S3*D*) (for further discussion, see *SI Text*).

Materials and Methods

Image Acquisition, Determination of Spatial Distribution, and Physical Location of Clustered DNA Damage. Images were captured by using an LSM 510 Meta laser scanning confocal microscope with a 63× 1.4-NA Plan-Apochromat oil immersion objective. Images were taken at *z*-sections (15–20 sections) of 0.5-μm intervals by using the 488-nm (EGFP-XRCC1), 543-nm (rhodamine), 633-nm (Alexa 633), and 405-nm (for DAPI) lasers. To avoid bleed-through effects in double/triple-staining experiments, each dye was scanned independently in a multitracking mode. To determine the spatial colocalization of 53BP1, XRCC1, and hOGG1 within the clustered DNA damage and the colocalization between clustered lesions and the heterochromatin, we used the colocalization function of the Imaris software (Bitplane, Inc.) as described (11). Other details of materials and methods are provided in *SI Text*.

ACKNOWLEDGMENTS. This work was supported by National Aeronautics and Space Administration Grants NNZ07AU42G and NNX11AC54G and National Institutes of Health Grant CA134991.

1. Nikjoo H, O'Neill P, Wilson WE, Goodhead DT (2001) Computational approach for determining the spectrum of DNA damage induced by ionizing radiation. *Radiat Res* 156:577–583.
2. Goodhead DT (1994) Initial events in the cellular effects of ionizing radiations: Clustered damage in DNA. *Int J Radiat Biol* 65:7–17.
3. Ward JF (1988) DNA damage produced by ionizing radiation in mammalian cells: identities, mechanisms of formation, and reparability. *Prog Nucleic Acid Res Mol Biol* 35:95–125.
4. Brenner DJ, Ward JF (1992) Constraints on energy deposition and target size of multiply damaged sites associated with DNA double-strand breaks. *Int J Radiat Biol* 61:737–748.
5. Blaisdell JO, Harrison L, Wallace SS (2001) Base excision repair processing of radiation-induced clustered DNA lesions. *Radiat Prot Dosimetry* 97:25–31.
6. Singleton BK, Griffin CS, Thacker J (2002) Clustered DNA damage leads to complex genetic changes in irradiated human cells. *Cancer Res* 62:6263–6269.
7. Hada M, Cucinotta FA, Gonda SR, Wu H (2007) mBAND analysis of chromosomal aberrations in human epithelial cells exposed to low- and high-LET radiation. *Radiat Res* 168:98–105.
8. Sedelnikova OA, et al. (2010) Role of oxidatively induced DNA lesions in human pathogenesis. *Mutat Res* 704:152–159.
9. Hall EJ, Hei TK (2003) Genomic instability and bystander effects induced by high-LET radiation. *Oncogene* 22:7034–7042.
10. Camacho CV, et al. (2010) Loss of p15/Ink4b accompanies tumorigenesis triggered by complex DNA double-strand breaks. *Carcinogenesis* 31:1889–1896.
11. Asaithamby A, et al. (2008) Repair of HZE-particle-induced DNA double-strand breaks in normal human fibroblasts. *Radiat Res* 169:437–446.
12. Falk M, Lukasova E, Kozubek S (2010) Higher-order chromatin structure in DSB induction, repair and misrepair. *Mutat Res* 704:88–100.
13. Tobias F, Durante M, Taucher-Scholz G, Jakob B (2010) Spatiotemporal analysis of DNA repair using charged particle radiation. *Mutat Res* 704:54–60.
14. Costes SV, Chiolo I, Pluth JM, Barcellos-Hoff MH, Jakob B (2010) Spatiotemporal characterization of ionizing radiation induced DNA damage foci and their relation to chromatin organization. *Mutat Res* 704:78–87.
15. Belyaev IY (2010) Radiation-induced DNA repair foci: Spatio-temporal aspects of formation, application for assessment of radiosensitivity and biological dosimetry. *Mutat Res* 704:132–141.
16. Goodarzi AA, Jeggo P, Lobrich M (2010) The influence of heterochromatin on DNA double strand break repair: Getting the strong, silent type to relax. *DNA Repair (Amst)* 9:1273–1282.
17. Goodarzi AA, et al. (2008) ATM signaling facilitates repair of DNA double-strand breaks associated with heterochromatin. *Mol Cell* 31:167–177.
18. Riballo E, et al. (2004) A pathway of double-strand break rejoining dependent upon ATM, Artemis, and proteins locating to gamma-H2AX foci. *Mol Cell* 16:715–724.
19. Terzoudi GI, Manola KN, Pantelias GE, Iliakis G (2005) Checkpoint abrogation in G2 compromises repair of chromosomal breaks in ataxia telangiectasia cells. *Cancer Res* 65:11292–11296.
20. Deckbar D, et al. (2007) Chromosome breakage after G2 checkpoint release. *J Cell Biol* 176:749–755.
21. Xu B, Kim ST, Lim DS, Kastan MB (2002) Two molecularly distinct G(2)/M checkpoints are induced by ionizing irradiation. *Mol Cell Biol* 22:1049–1059.
22. Holley WR, Chatterjee A (1996) Clusters of DNA induced by ionizing radiation: formation of short DNA fragments. I. Theoretical modeling. *Radiat Res* 145:188–199.
23. Urushibara A, et al. (2008) LET dependence of the yield of single-, double-strand breaks and base lesions in fully hydrated plasmid DNA films by 4He(2+) ion irradiation. *Int J Radiat Biol* 84:23–33.
24. Nikjoo H, Uehara S, Wilson WE, Hoshi M, Goodhead DT (1998) Track structure in radiation biology: Theory and applications. *Int J Radiat Biol* 73:355–364.
25. Paap B, Wilson DM, 3rd, Sutherland BM (2008) Human abasic endonuclease action on multilesion abasic clusters: Implications for radiation-induced biological damage. *Nucleic Acids Res* 36:2717–2727.
26. Costes SV, et al. (2007) Image-based modeling reveals dynamic redistribution of DNA damage into nuclear sub-domains. *PLOS Comput Biol* 3:e155.
27. Holt SM, Scemama JL, Panayiotidis MI, Georgakilas AG (2009) Compromised repair of clustered DNA damage in the human acute lymphoblastic leukemia MSH2-deficient NALM-6 cells. *Mutat Res* 674:123–130.
28. Löbrich M, Jeggo PA (2007) The impact of a negligent G2/M checkpoint on genomic instability and cancer induction. *Nat Rev Cancer* 7:861–869.